



NAVAL POSTGRADUATE SCHOOL

MONTEREY, CALIFORNIA

THESIS

EFFECTS OF VERTICAL SHEAR ON ARCTIC DOUBLE DIFFUSIVE STAIRCASES

by

William D. Tubbs

December 2018

Thesis Advisor:
Second Reader:

Timour Radko
Justin M. Brown

Approved for public release. Distribution is unlimited.

THIS PAGE INTENTIONALLY LEFT BLANK

REPORT DOCUMENTATION PAGE			<i>Form Approved OMB No. 0704-0188</i>	
Public reporting burden for this collection of information is estimated to average 1 hour per response, including the time for reviewing instruction, searching existing data sources, gathering and maintaining the data needed, and completing and reviewing the collection of information. Send comments regarding this burden estimate or any other aspect of this collection of information, including suggestions for reducing this burden, to Washington headquarters Services, Directorate for Information Operations and Reports, 1215 Jefferson Davis Highway, Suite 1204, Arlington, VA 22202-4302, and to the Office of Management and Budget, Paperwork Reduction Project (0704-0188) Washington, DC 20503.				
1. AGENCY USE ONLY (Leave blank)		2. REPORT DATE December 2018		3. REPORT TYPE AND DATES COVERED Master's thesis
4. TITLE AND SUBTITLE EFFECTS OF VERTICAL SHEAR ON ARCTIC DOUBLE DIFFUSIVE STAIRCASES			5. FUNDING NUMBERS RQGPQ	
6. AUTHOR(S) William D. Tubbs				
7. PERFORMING ORGANIZATION NAME(S) AND ADDRESS(ES) Naval Postgraduate School Monterey, CA 93943-5000			8. PERFORMING ORGANIZATION REPORT NUMBER	
9. SPONSORING / MONITORING AGENCY NAME(S) AND ADDRESS(ES) N/A			10. SPONSORING / MONITORING AGENCY REPORT NUMBER	
11. SUPPLEMENTARY NOTES The views expressed in this thesis are those of the author and do not reflect the official policy or position of the Department of Defense or the U.S. Government.				
12a. DISTRIBUTION / AVAILABILITY STATEMENT Approved for public release. Distribution is unlimited.			12b. DISTRIBUTION CODE A	
13. ABSTRACT (maximum 200 words) <p>Double diffusive convection through Arctic staircases has been shown to play a role in the melting of Arctic sea ice. However, there have been no studies exploring the effects of shear on these staircases. We simulated these staircases numerically in the presence of vertical shear to determine its effects on the heat flux and structure of the staircases. Results from this study imply the heat flux increases 20% to 30% above cases with no shear. Simulations yielded an unexpected result that, with the addition of shear, a turbulent motion occurs inside the interfaces between staircase layers that typically are devoid of vertical motion in the absence of shear. These features are attributed to the recently discovered thermohaline-shear instability. An investigation of turbulent kinetic energy indicates that the intensity of this instability may depend on both Richardson number and density ratio. Understanding the effects of vertical shear on the staircases, and in particular on the associated heat flux, may lead to more accurate mixing parameterizations in global climate models.</p>				
14. SUBJECT TERMS double diffusion, arctic staircases, heat flux, diffusive convection, Arctic Ocean modeling			15. NUMBER OF PAGES 55	
			16. PRICE CODE	
17. SECURITY CLASSIFICATION OF REPORT Unclassified	18. SECURITY CLASSIFICATION OF THIS PAGE Unclassified	19. SECURITY CLASSIFICATION OF ABSTRACT Unclassified	20. LIMITATION OF ABSTRACT UU	

THIS PAGE INTENTIONALLY LEFT BLANK

Approved for public release. Distribution is unlimited.

**EFFECTS OF VERTICAL SHEAR ON ARCTIC DOUBLE DIFFUSIVE
STAIRCASES**

William D. Tubbs
Lieutenant Commander, United States Navy
BS, State University of New York Maritime College, 2008
MS, University of Southern Mississippi, 2014

Submitted in partial fulfillment of the
requirements for the degree of

**MASTER OF SCIENCE IN METEOROLOGY AND PHYSICAL
OCEANOGRAPHY**

from the

**NAVAL POSTGRADUATE SCHOOL
December 2018**

Approved by: Timour Radko
Advisor

Justin M. Brown
Second Reader

Peter C. Chu
Chair, Department of Oceanography

THIS PAGE INTENTIONALLY LEFT BLANK

ABSTRACT

Double diffusive convection through Arctic staircases has been shown to play a role in the melting of Arctic sea ice. However, there have been no studies exploring the effects of shear on these staircases. We simulated these staircases numerically in the presence of vertical shear to determine its effects on the heat flux and structure of the staircases. Results from this study imply the heat flux increases 20% to 30% above cases with no shear. Simulations yielded an unexpected result that, with the addition of shear, a turbulent motion occurs inside the interfaces between staircase layers that typically are devoid of vertical motion in the absence of shear. These features are attributed to the recently discovered thermohaline-shear instability. An investigation of turbulent kinetic energy indicates that the intensity of this instability may depend on both Richardson number and density ratio. Understanding the effects of vertical shear on the staircases, and in particular on the associated heat flux, may lead to more accurate mixing parameterizations in global climate models.

THIS PAGE INTENTIONALLY LEFT BLANK

TABLE OF CONTENTS

I.	INTRODUCTION.....	1
II.	METHODOLOGY	7
A.	MODEL	7
B.	INITIAL CONDITIONS.....	8
III.	RESULTS: HEAT FLUXES.....	13
A.	COMPARATIVE ANALYSIS OF 3D VS. 2D SIMULATIONS.....	13
B.	COMPARATIVE ANALYSIS OF SIMULATIONS WITH VARIOUS SHEAR MODELS.....	15
1.	Constant Shear	15
2.	Oscillating Shear	18
3.	Stochastic Shear	22
C.	EFFECTS OF SHEAR ON THE LAYER STRUCTURE	23
IV.	RESULTS: ENERGETICS.....	27
A.	CONSTANT SHEAR.....	27
B.	OSCILLATING SHEAR.....	28
C.	STOCHASTIC SHEAR.....	29
V.	SUMMARY	31
A.	CONCLUSIONS	31
B.	RECOMMENDATIONS.....	32
	LIST OF REFERENCES	33
	INITIAL DISTRIBUTION LIST	37

THIS PAGE INTENTIONALLY LEFT BLANK

LIST OF FIGURES

Figure 1.	Variations in sea ice melt. Source: Maslowski et al. (2012).....	1
Figure 2.	Three mechanisms contribute to sea ice melt. Source: Turner (2010).	2
Figure 3.	Under ice temperature profile. Source: Neal et al. (1969).....	4
Figure 4.	Constant shear setup.	9
Figure 5.	Oscillating shear setup.	9
Figure 6.	Stochastic shear setup.	10
Figure 7.	3D Shear simulation.....	14
Figure 8.	3D vs. 2D heat flux series.	15
Figure 9.	Heat flux vs. Richardson number.....	18
Figure 10.	Oscillating shear heat flux series.	21
Figure 11.	C vs. density ratio.	23
Figure 12.	W velocity comparison.	24
Figure 13.	Shear vs. no-shear series.	24
Figure 14.	Coherent vs. disrupted layers.....	25
Figure 15.	TKE series: Constant shear.....	28
Figure 16.	TKE series: Oscillating shear.....	29
Figure 17.	Stochastic simulation.	30

THIS PAGE INTENTIONALLY LEFT BLANK

LIST OF TABLES

Table 1.	Constant shear simulations.	16
Table 2.	Oscillating and stochastic shear simulations.....	20

THIS PAGE INTENTIONALLY LEFT BLANK

LIST OF ACRONYMS AND ABBREVIATIONS

AIWEX	Arctic Internal Wave Experiment
DNS	Direct Numerical Simulation
DoD	Department of Defense
HPC	High Performance Computing
ITP	Ice-Tethered Profiler
MITgcm	Massachusetts Institute of Technology general circulation model
NAME	Naval Postgraduate School Arctic Modelling Effort
NPS	Naval Postgraduate School
NSIDC	National Snow and Ice Data Center
SHEBA	Surface Heat Budget of the Arctic Ocean

THIS PAGE INTENTIONALLY LEFT BLANK

ACKNOWLEDGMENTS

I would like to thank my advisor, Dr. Timour Radko. His boundless energy and positive mental attitude motivated me to press harder and complete this monumental task. His knowledge of modelling and the subject matter pushed me over countless hurdles. It was an honor working for the man who literally wrote the book on double-diffusive convection.

I would like to thank Dr. Justin Brown. There would be no thesis if he hadn't been available for support—the countless weeks of not only attempting to help me understand the material but also patiently, and painfully, watching me write programming code in Matlab and on the HPCs. Lastly, for being the translation matrix between Dr. Radko and myself.

I would like to thank “Team Timour,” Dave, James, Rino, and Marco. Although the topics were quite different, we pushed through endless simulations and programming code errors.

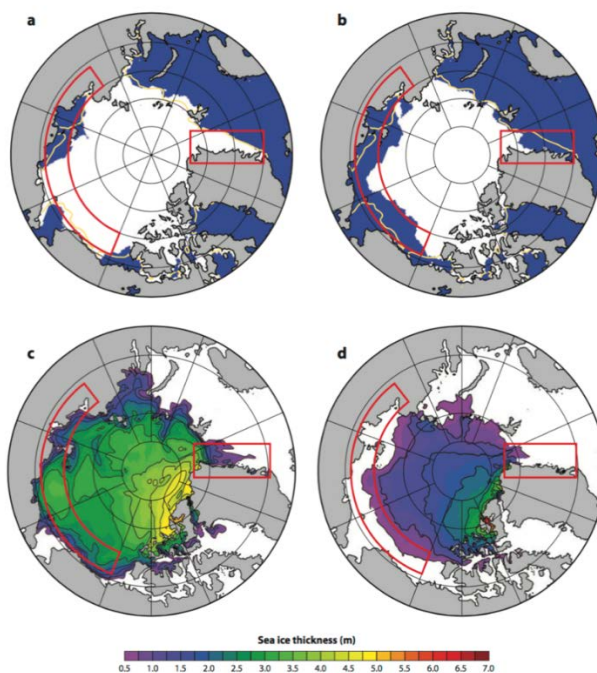
This research was supported in part by a grant of computer time from the DoD HPCMP at the ERDC. Naval Postgraduate School HPC was used to run a vast number of simulations, MATLAB software for plots, and calculations.

Lastly, I would like to thank my wife, Nicole, and my family, as they have supported my time away from home while completing this research.

THIS PAGE INTENTIONALLY LEFT BLANK

I. INTRODUCTION

The global community, specifically nations that border the Arctic Ocean, has been closely watching the mean reduction in sea ice thickness and extent in the Arctic Circle. These reductions may open opportunities for unearthing previously unreachable natural resources and opening new shipping routes for delivering products overseas. A number of studies have examined satellite records which indicate a decreasing trend of sea ice concentration and extent (Maslowski et al. 2012; Stroeve and Maslowski 2008; Stroeve et al. 2011a), see Figure 1, which shows that throughout the basin, sea ice thickness reductions are in excess of 2m. Accurately predicting the rate of sea ice melt depends on understanding several physical processes, including the heat flux through complex thermal features beneath the mixed layer of the Arctic.

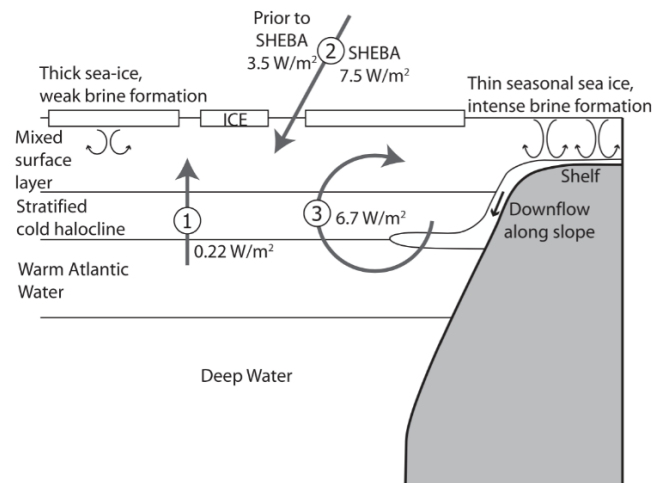


Comparison of (a, b) observed September ice extent from National Snow and Ice Data Center (NSIDC) with (c, d) Naval Postgraduate School Arctic Modeling Effort (NAME) modeled ice extent and thickness (a, c) 1988 and (b, d) 2002.

Figure 1. Variations in sea ice melt. Source: Maslowski et al. (2012).

The Arctic Ocean is comprised of various water masses whose structure determine the dynamical and thermal processes that govern the sea ice melt. It is sourced by Atlantic water, Pacific water (western Arctic only), river runoff, and sea/land ice melt. The Atlantic water is warm and salty as compared to the cooler, fresher water from ice melt, and subducts beneath it to create a well-mixed, relatively fresh, and cold layer at the surface and denser, warm, and salty layer underneath separated by a well-defined pycnocline. Because of this unique structure, there are various modes of heat transport that contribute to sea ice reduction.

The predominant heat transport into the Arctic sea ice can be identified as three distinct processes that were categorized in Turner (2010) and are shown in Figure 2. He analyzed data provided from an observational study conducted by Perovich and Elder (2002) called SHEBA (Surface Heat Budget of the Arctic Ocean), a laboratory study by Wells and Wettlaufer (2007), and a diffusive convection study by Kelley (1984). His analysis suggests that diffusive convection between water-masses of Atlantic and Pacific origin transports heat upward at the rate which is sufficient to substantially influence the sea-ice coverage and the melt rate. Therefore, this research will primarily focus on heat transport through double-diffusive convection.



(1) Upward double diffusive heat transport from the Atlantic layer, (2) heat flux from the atmosphere into the turbulent mixed layer and then to ice, and (3) mean surface heat flux over the entire Arctic Ocean required to balance the net input of heat from the Atlantic layer.

Figure 2. Three mechanisms contribute to sea ice melt. Source: Turner (2010).

Double diffusive convection is a phenomenon that occurs in a fluid with two or more components with different molecular diffusivities (Stern 1960; Walin 1964). In the ocean, the relevant density components are the salinity and temperature. Since heat diffuses two orders of magnitude faster than salt, various water-masses in the ocean are strongly susceptible to double-diffusive convection. Double-diffusion is known to be controlled by the density ratio

$$R_\rho = \frac{\beta \partial S / \partial z}{\alpha \partial T / \partial z}, \quad (1)$$

where (T, S) represent fluid temperature and salinity and (α, β) are the constant expansion/contraction coefficients. The density ratio, R_ρ , describes the contribution to density caused by the salinity over the corresponding contribution caused by temperature. This quantity varies in the arctic region in the range of $2 \leq R_\rho \leq 7$ (Padman et al. 1987). Double-diffusion can be classified into two distinct regimes: salt fingering, typically found in tropical and mid-latitude regions where warm salty water overlays cool fresher water, and diffusive convection, found in the Arctic and Antarctic regions where cool fresher water overlays warm salty water. For more information on salt fingering, refer to Radko (2013). Diffusive convection occurs where the fluid is hydrostatically stable despite an unstable thermogradient and is known to establish the well-defined thermohaline staircases (Neal et al. 1969 and Timmermans et al. 2008).

These thermohaline staircases are comprised of alternating isothermal/isohaline layers and interfaces of steep thermal/haline gradients at depth. Typically, overturning circulation occurs in these layers and the associated interfaces will remain relatively motionless while heat and salt diffuse through them. Figure 3 shows an under-ice temperature profile identifying such a staircase. Analogous salinity profiles closely resemble the temperature in such regions. In the Arctic, the mean heat transport, or flux, through these staircases is was estimated to be on the order of $0.22 \frac{W}{m^2}$ as shown in Figure 2. This estimate (Turner 2010) was made based on the extrapolation of laboratory experiments. Flanagan et al. (2013) calculated the heat flux, at various density ratios, through these staircases using direct numerical simulations (DNS). He deduced that at

lower density ratios, there resulted in higher heat fluxes. However, there have been no systematic investigations into the effects of vertical shear, which is ubiquitous in all regions of the world's oceans.

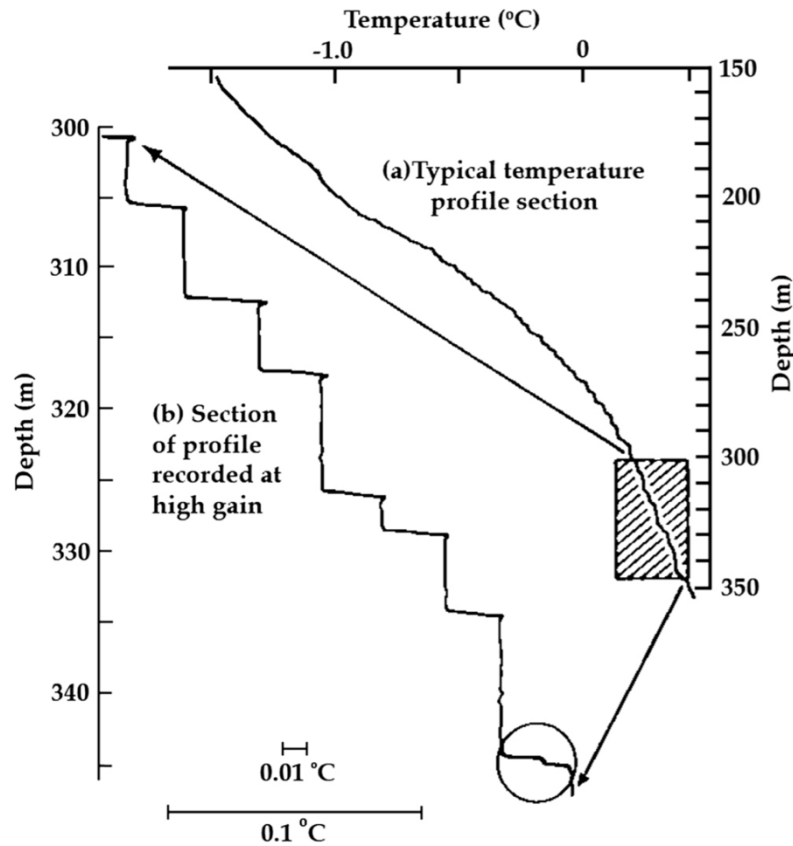


Figure 3. Under ice temperature profile. Source: Neal et al. (1969).

Shear in its simplest form occurs in any region where the gradient of the velocity is not zero. In the deep ocean where atmospheric forcing is not a significant factor, shear is typically caused by internal waves that are generated by tidal forcing displacing water over the seafloor. Levine et al. (1987) conducted the Arctic Internal Wave Experiment (AIWEX) in order to compare the frequencies of internal waves in the Arctic to those at lower latitudes. The results from this study provided a shear spectrum that is used in some of the time-varying shear simulations conducted for this research.

Oceanic shear is a critical component for stability throughout the water column. The strength of shear is traditionally quantified using the Richardson number Ri , defined as

$$Ri = \frac{N^2}{(\partial u / \partial z)^2}, \quad (2)$$

which is the square of the ratio of the Brunt-Väisälä Buoyancy Frequency (N) to the vertical shear rate ($\partial u / \partial z$), the former of which is given by

$$N^2 = \frac{g}{\rho_o} \frac{\partial \rho}{\partial z}, \quad (3)$$

where g is Earth's gravitational constant.

Two major sources of small-scale mixing in the ocean interior are Kelvin-Helmholtz instability and double-diffusion. A fluid which is known to be dynamically stable in regards to Kelvin-Helmholtz instability if $Ri > \frac{1}{4}$. However, according to Brown and Radko (2018, in press), two-component fluids could still be unstable with regard to the so-called thermohaline-shear instability even when $Ri > \frac{1}{4}$.

With shear clearly observed in the Arctic and diffusive convection identified as a source of heat flux under the ice, this study uses numerical simulations to analyze the effect of shear on the arctic staircase structure and heat flux from diffusive convection. The interfacial dynamics change substantially in the presence of shear, resulting in strong variation in velocity across diffusive interfaces. A series of Direct Numerical Simulations (DNS) performed in the course of this investigation led to the conclusion that, as compared to simulations without shear, there was a general increase in the mean heat flux when a constant or oscillating shear was applied. Additionally, as the density ratio increased, the magnitude of the heat flux also increased. The stochastic-shear simulations produced a negligible difference as compared to the corresponding no-shear simulations. All shear simulations revealed intense mixing at the interfaces that we attribute to thermohaline-shear instabilities. As the shear increases, the turbulent kinetic energy increases as well. We find in our simulations that the addition of shear to diffusive layers' results in increased activity at the interfaces.

This thesis is structured as follows. The description of the model, governing equations, and the setup of numerical experiments is offered in Chapter II. Chapter III presents the key numerical results; particular attention is given to the analysis of differences and similarities between two- and three-dimensional simulations. Chapter IV discusses the energetics of the interaction between shear and diffusive convection, and Chapter V contains concluding remarks.

II. METHODOLOGY

A. MODEL

Our numerical simulations were conducted using the Massachusetts Institute of Technology General Circulation Model (MITgcm). This is an oceanic and atmospheric model that has a non-hydrostatic capability and that uses finite-volume techniques to discretize the system. Yielding intuitive discretization, this model is ideal for simulations from the micro to global scales. For further information regarding the architecture and development, the reader should refer to Hill and Marshall (1995), Marshall et al. (1997), Adcroft et al. (1997), Marshall et al. (1998), and Adcroft and Marshall (1999).

The governing equations solved by MITgcm include the Boussinesq momentum equations for incompressible and irrotational fluid in the presence of vertical shear

$$\frac{\partial \mathbf{u}}{\partial t} + \mathbf{u} \cdot \nabla \mathbf{u} = -\frac{\nabla p}{\rho_o} - g \frac{\rho - \rho_o}{\rho_o} \hat{\mathbf{z}} + \nu \nabla^2 \mathbf{u}, \quad (4)$$

where \mathbf{u} is the non-divergent velocity field, p is the dynamic pressure, ν is the kinematic viscosity, ρ is the density, and ρ_o is a reference density (Radko 2013). The effect of the Earth's rotation is assumed negligible for double diffusion as the system features are of meter scales. For these simulations, $\nu = 1 \times 10^{-6} \frac{m^2}{s}$; $g = 9.81 \frac{m}{s^2}$.

The advection-diffusion temperature and salinity equations are

$$\frac{\partial T}{\partial t} + \mathbf{u} \cdot \nabla T = K_T \nabla^2 T \quad (5)$$

$$\frac{\partial S}{\partial t} + \mathbf{u} \cdot \nabla S = K_S \nabla^2 S, \quad (6)$$

where, K_T and K_S represents the molecular diffusivity coefficients for T and S . The thermal diffusivity is larger than the saline diffusivity, $K_T > K_S$, and these two quantities are commonly related using their ratio, $\tau \equiv K_S/K_T$, which is found to be roughly 0.005 in the Arctic. Due to the resolution limits of the model, these simulations used a τ of 0.1 with $K_T = 1.5 \times 10^{-6} \frac{m^2}{s}$ and $K_S = 1.5 \times 10^{-7} \frac{m^2}{s}$. The continuity equation is

$$\nabla \cdot \mathbf{u} = 0, \quad (7)$$

where the fluid is assumed incompressible. The equation of state has been linearized and is given by

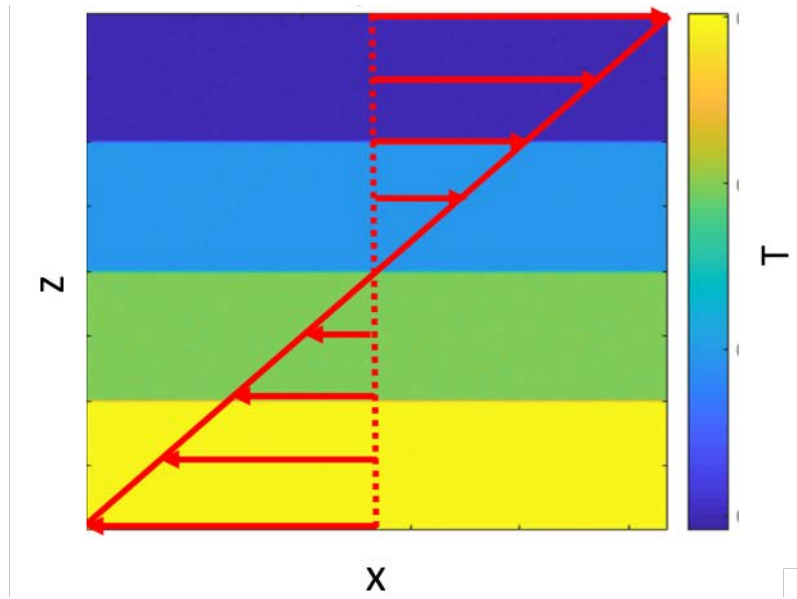
$$\frac{\rho - \rho_o}{\rho_o} = -\alpha(T - T_o) + \beta(S - S_o) , \quad (8)$$

where (T_o, S_o) are the reference temperature and salinity. For these simulations, $\alpha = 1 \times 10^{-4} \text{C}^{-1}$; $\beta = 7.5 \times 10^{-4} \text{psu}^{-1}$.

The simulation setup assumed diffusive convective staircases had been established within a domain with dimensions of: 3D $\sim 1.6\text{m}$ by $\sim 1.3\text{m}$ by $\sim 2.5\text{m}$ (x, y, z), resolved by 448 by 440 by 800 mesh, 2D $\sim 1.6\text{m}$ by $\sim 2.5\text{m}$ (x, z), resolved by 448 by 1 by 800 mesh. The box was subsequently divided vertically into four stratified horizontal layers of equal thickness with free-slip impermeable boundaries at the top and bottom of the domain. The horizontal boundaries were set to be periodic to reflect the effectively unbounded nature of the open ocean.

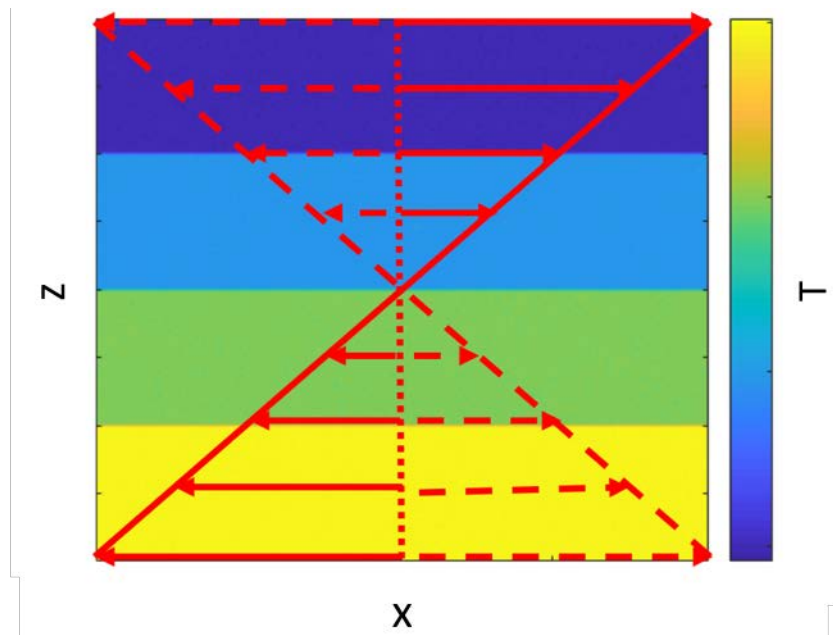
B. INITIAL CONDITIONS

The initial conditions were such that the bottom of the computational domain was warmer, by 0.2°C , and saltier, by 0.06psu , than the top. This setup reflects the structure of thermohaline staircases and is representative of the region in between the warm Atlantic water and the Pacific water or Arctic mixed layer. The shear simulations are represented in Figures 4, 5, and 6.



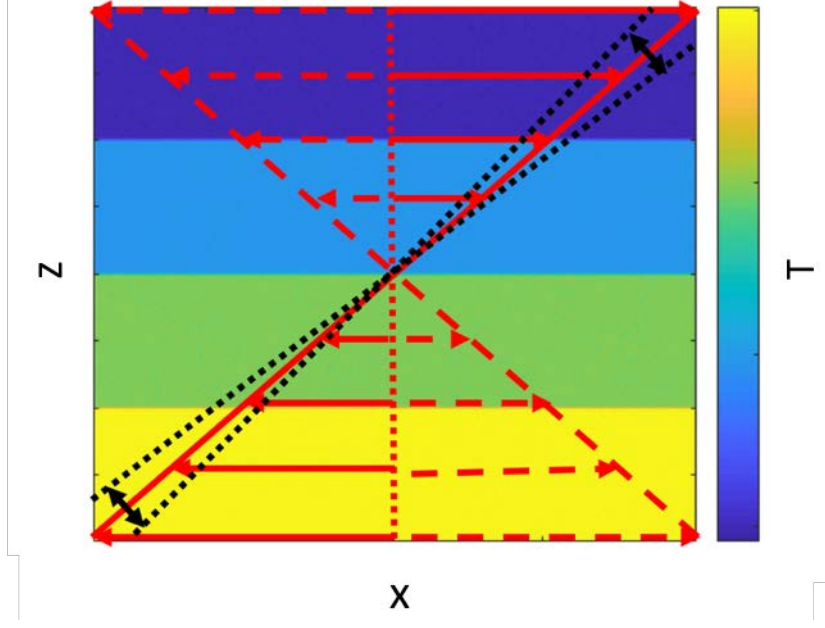
Arrows indicate magnitude and direction of applied shear.

Figure 4. Constant shear setup.



Arrows indicate magnitude and direction of applied shear.

Figure 5. Oscillating shear setup.



Red arrows indicate magnitude and direction of applied shear. Black lines and arrows indicate a wobble.

Figure 6. Stochastic shear setup.

The simulations performed in this study could be classified into four distinct categories: without vertical shear, with a constant shear, with an oscillating shear, and with a stochastic shear forcing. The velocity of the background field is given by \bar{u} and is only in the x-direction. In order to excite a shear component in the simulations, various forms of \bar{u} were added to the simulations. For the constant shear simulations, the externally imposed shear is given by

$$\bar{u} = \left(z \frac{\partial \bar{u}}{\partial z} + u_o \right), \quad (9)$$

where $\frac{\partial \bar{u}}{\partial z}$ is constant. For oscillating shear, this expression is instead

$$\bar{u} = \left(z \frac{\partial \bar{u}}{\partial z} + u_o \right) \cos(2\pi f), \quad (10)$$

where $\cos(2\pi f)$ term represents the oscillation. Lastly, for stochastic shear, the corresponding expression is

$$\bar{u} = \sum_{i=1}^N \left(z \frac{\partial \bar{u}}{\partial z} + u_o \right) \cos(2\pi f_i + \varphi_i) \frac{f_i^r}{f_1^r}, f_i = [f_1, f_N], \quad (11)$$

where the frequencies are evenly spaced in logarithmic space, r is the spectral power and is set to -0.5 (Levine et al. 1987), and N is the total number of shear modes and is set to 10.

THIS PAGE INTENTIONALLY LEFT BLANK

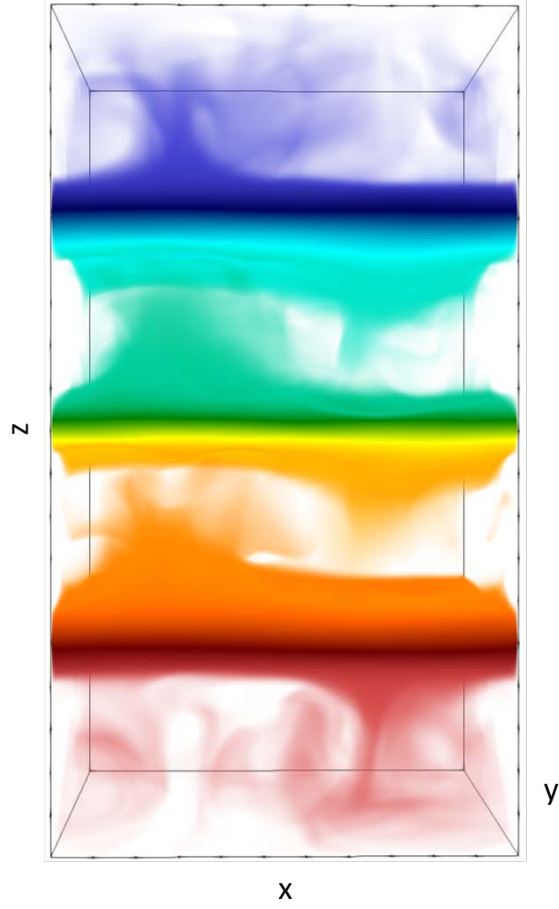
III. RESULTS: HEAT FLUXES

We simulated 18 diffusive layered systems using DoD HPC and NPS HPC systems, three “no-shear,” nine “constant-shear,” four “oscillating-shear,” one “stochastic-shear,” and one 3D “constant-shear.” The constant- and no-shear simulations were performed using $R_\rho = [3,5,7]$ and $Ri = [\infty, 40, 10, 5]$, where $Ri = \infty$ represents no-shear simulations. The oscillating-shear simulations were set up with a constant oscillation frequency that varied from the inertial frequency in the first simulation up to the buoyancy frequency in the last. The stochastic simulation represented the range of frequencies from inertial to buoyancy with spectral power dependence based on measurements by Levine et al. (1987).

First, a comparison between the 2D and 3D simulations was conducted to justify using 2D simulations as a representation of actual ocean dynamics. Then each simulation was compared to the no-shear simulations in order to determine shear-related effects on both the heat flux and layer structure. Comparisons were also made between the various density ratios, Richardson numbers, and shear regimes.

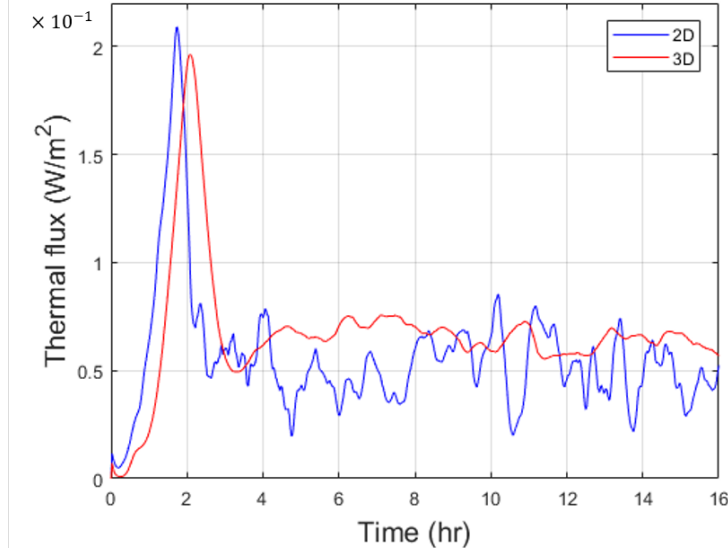
A. COMPARATIVE ANALYSIS OF 3D VS. 2D SIMULATIONS

Three-dimensional simulations (i.e., Figure 7), have a high computational cost, requiring significantly more time to complete, and therefore, the majority of the simulations for this research were conducted in 2D. However, a 3D, constant shear, high Richardson number simulation was compared to a 2D simulation of the same conditions to ensure that there were no significant differences. Flanagan et al. (2013) previously concluded that 2D numerical diffusive convection simulations performed within 10% of the 3D simulations with the same parameters. The two simulations compared in Figure 8 were performed for $R_\rho = 3$ and $Ri = 40$, resulting in the 3D simulation having a 30% greater heat flux.



$R_\rho = 3$ $Ri = 40$ constant shear 3D simulation indicating the haline flux between the layers.

Figure 7. 3D Shear simulation.



3D simulation (red) of thermal flux over time as compared to 2D simulation (blue) with the same parameters.

Figure 8. 3D vs. 2D heat flux series.

The results are comparable to those of Flanagan et al. (2013), who used periodic boundary conditions in all dimensions and $\tau = 0.005$, whereas simulations in Figures 7 and 8 used impermeable boundary conditions on the top and bottom and $\tau = 0.1$. These differences may account for the higher heat flux in Flanagan et al. (2013).

B. COMPARATIVE ANALYSIS OF SIMULATIONS WITH VARIOUS SHEAR MODELS

1. Constant Shear

Nine constant-shear simulations were conducted with R_ρ values of 3, 5, and 7 and Richardson numbers of 40, 10, and 5. These simulations had constant external shear applied to the system. The only difference between the following simulations are the values of density ratio and shear. These simulations were then compared to the “no-shear” simulations of the same R_ρ to quantify the differences in heat flux. These simulations are summarized in Table 1. All 3D simulations were performed in the computational domain of $\sim 1.6\text{m}$ by $\sim 1.3\text{m}$ by $\sim 2.5\text{m}$ (x, y, z), resolved by 448 by 440 by 800 mesh, 2D simulations of $\sim 1.6\text{m}$ by $\sim 2.5\text{m}$ (x, z), resolved by 448 by 1 by 800, and the overall vertical temperature variation of $\Delta T = 0.2^\circ\text{C}$.

Table 1. Constant shear simulations.

Constant Shear Simulations									
R_ρ	Ri	$\frac{\partial \bar{u}}{\partial z}$ (Hz)	F_T (W/m ²)	$F_T - F_{T,0}$	σ_T	F_S (psu m/s)	$F_S - F_{S,0}$	σ_S	γ
3	INF	0	0.02414	0	0.00521	3.2554E-10	0	1.1359E-10	0.4001
3	40	0.009	0.02634	0.0022	0.00465	3.3647E-10	1.0930E-11	1.2418E-10	0.3789
3	10	0.017	0.03015	0.00601	0.00724	4.1018E-10	8.4640E-11	2.8235E-10	0.4036
3	5	0.025	0.03148	0.00734	0.01111	4.4252E-10	1.1698E-10	6.6515E-10	0.4169
5	INF	0	0.0162	0	0.00363	2.1324E-10	0	7.8081E-11	0.3904
5	40	0.012	0.0195	0.0033	0.00401	2.6124E-10	4.8000E-11	1.0013E-10	0.3974
5	10	0.025	0.02064	0.00444	0.0056	2.7933E-10	6.6090E-11	4.9231E-10	0.4015
5	5	0.035	0.02317	0.00697	0.01281	4.3046E-10	2.1722E-10	1.5864E-10	0.5512
7	INF	0	0.01365	0	0.00284	1.7757E-10	0	5.8369E-11	0.3858
7	40	0.015	0.01758	0.00393	0.00373	2.8295E-10	1.0538E-10	1.3228E-10	0.4774
7	10	0.03	0.01278	-0.00087	0.00802	1.6732E-10	-1.0250E-11	1.6310E-09	0.3884
7	5	0.043	0.11308	0.09943	0.33623	1.8913E-08	1.8735E-08	8.2795E-08	4.9613

Fluxes in Table 1 were calculated using the following expressions:

$$F_H = \rho_o c_p \langle wT \rangle \quad (12)$$

$$F_S = \rho_o c_p \langle wS \rangle \quad (13)$$

where ρ_o is the mean density; c_p is the specific heat at constant pressure; and $\langle w[TS] \rangle$ are the spatial average of the vertical velocity times the temperature or salinity taken from the interior part of the computational domain in order to minimize the effects of the top and bottom boundary conditions. The heat fluxes were averaged over the temporal interval between 10 hours to 25 hours from the beginning of the experiment. This range provides enough time for the simulations to reach a state of quasi-equilibrium and provide a significant amount of data for analysis. The flux ratio, which is used to determine whether the fluxes are associated with double diffusive convection, is calculated as follows:

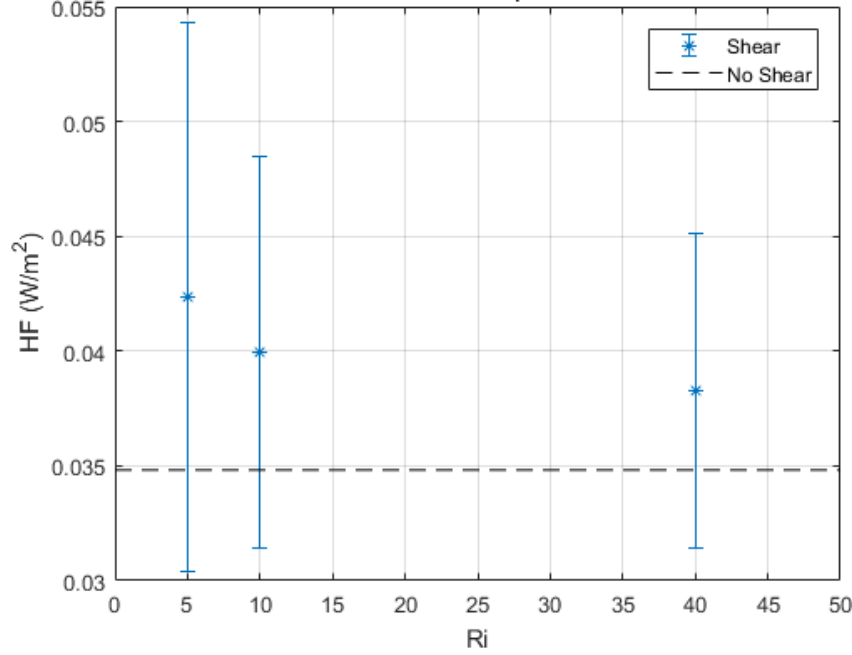
$$\gamma = \frac{\beta \langle wS \rangle}{\alpha \langle wT \rangle} \quad (14)$$

where $\gamma < 1$ suggests that the fluxes are indeed a result of diffusive convection.

Generally, the simulations indicated a slight increase in F_T as compared to the heat flux for the simulations without shear, $F_{T,0}$. Specifically, the $R_\rho = (3,5)$ simulations showed flux increases of 20% and 30%, respectively. With $\gamma < 1$, we can say with confidence that this change could be caused by diffusive convection. With regard to the systematic shear-induced increase in heat flux, it should be noted that the salt finger form of double-diffusive convection exhibits the opposite trend. Several studies (e.g., Smyth and Kimura 2007; Radko 2010; Radko et al. 2015) have shown that shear can reduce fingering fluxes by a factor of two or more.

Another identified trend for these simulations is that as the Richardson number decreases, F_T increases. For example, for $R_\rho = 3$ from $Ri = \infty$ to $Ri = 5$, F_T increases from 0.024 to 0.031, which can be seen in Figure 9. Although the $R_\rho = 7$ simulations with $Ri = \infty$ and $Ri = 40$ follow these identified trends, the $Ri = (10,5)$ cases do not. This suggests that processes other than diffusive convection may have occurred. Additionally, F_T from shear simulations of all density ratios had much larger fluctuations about the mean

when compared to simulations without shear, indicating an increase in turbulent motion throughout the layers.



Mean heat flux produced from added shear versus the no shear condition (dashed line); the plotted error bars indicate the standard deviation about the mean and are not an estimate of the error.

Figure 9. Heat flux vs. Richardson number.

2. Oscillating Shear

Four oscillating-shear simulations were evaluated against the constant-shear regime and no-shear simulations. The initial temperature and salinity fields were the same as those from the constant shear simulation of $R_\rho = 3$ and $Ri = 10$. According to Cole et al. (2014), ice-tethered profile measurements give a rough estimate of $Ri = 10$ throughout a large portion of the Arctic, so, to isolate the effect of an oscillating shear, the simulations were constructed using values of $R_\rho = 3$ and $Ri = 10$ with various frequencies, which are taken to be representative. The assumption is made that the results will be analogous for other density ratios and Richardson numbers. The frequencies selected are as follows: simulation A, inertial frequency ($1.16 \times 10^{-5} Hz$); simulation B, half an order of

magnitude greater than the inertial frequency ($5.79 \times 10^{-5}\text{Hz}$); simulation C, an order of magnitude greater than the inertial frequency ($1.16 \times 10^{-4}\text{Hz}$); and simulation D, buoyancy frequency (0.0069 Hz).

Table 2. Oscillating and stochastic shear simulations.

Oscillating and Stochastic Shear Simulations										
f (Hz)		R_ρ	Ri	F_T (W/m ²)	$F_T - F_{T,0}$	σ_T	F_S (psu m/s)	$F_S - F_{S,0}$	σ_S	γ
No Shear	0	3	INF	0.02414	0	0.00521	3.2554E-10	0	1.1359E-10	0.4001
A	1.1570E-05	3	10	0.03078	0.00664	0.01081	4.2673E-10	1.0119E-10	4.6916E-10	0.4113
B	5.7850E-05	3	10	0.03481	0.01067	0.02004	5.5387E-10	2.2833E-10	7.6922E-10	0.4719
C	1.1570E-04	3	10	0.02574	0.0016	0.00726	2.9376E-10	-3.1780E-11	1.5969E-10	0.3386
D	0.0069	3	10	0.0238	-0.00034	0.07924	3.0054E-10	-2.5000E-11	8.0799E-09	0.3746
Stochastic	1.2E-5 to 1.1E-3	3	10	0.02316	-0.00762	0.01484	3.70E-10	-5.6540E-11	8.52E-10	0.4741

Oscillating and Stochastic shear simulations where A is the inertial frequency, B is half an order of magnitude greater than the inertial frequency, C is an order of magnitude greater than the inertial frequency, and D is the buoyancy frequency. Stochastic simulation uses a range of frequencies from the inertial frequency to a value less than the buoyancy frequency.

These simulations yielded F_T deviations from the no-shear case that ranged from negligible change (simulation D) to a maximum of 0.01 W/m^2 (simulation B) as shown in Table 2 and displayed over-time in Figure 10. Heat flux values were larger for the oscillating simulations, as compared to no shear simulations, except when the buoyancy frequency shear was applied. There also appeared to be a frequency where heat flux was maximized at B. A reasonable explanation for the buoyancy frequency phenomena is that the simulations rigid top and bottom boundary conditions inhibit large-scale vertical motion. According to Brown and Radko (2018, in press), when shear oscillates at or near the buoyancy frequency, there should be a distinct and amplifying vertical velocity signal occurring over the entire vertical domain. With the rigid boundaries, this formation is unable to develop properly.

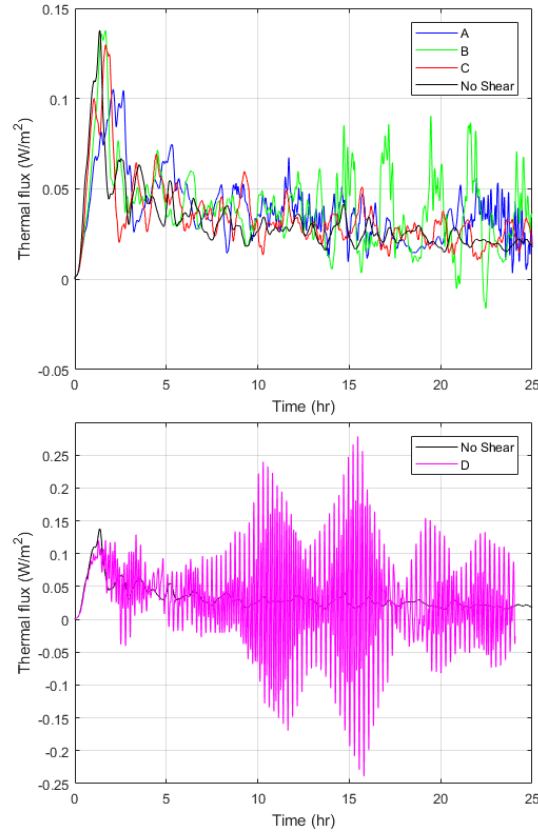


Figure 10. Oscillating shear heat flux series.

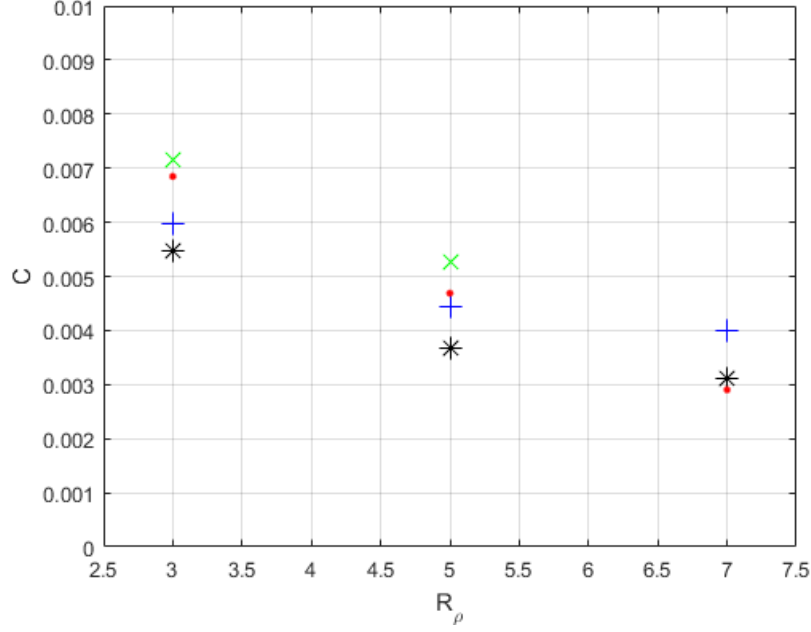
3. Stochastic Shear

One stochastic simulation, shown in Table 2, was conducted for comparison with constant shear and no-shear experiments. The frequencies for the stochastic shear simulation range from the inertial frequency to buoyancy frequency. With this frequency range, there was an expectation of an increase in F_T similar to the behavior of the oscillating simulations. However, the resulting F_T had a negligible difference when compared to the simulation without shear. This suggests that stochastic shear is more likely to maintain layer coherence.

In addition to the heat flux, another commonly used measure of the intensity of vertical mixing in thermohaline staircases is afforded by the coefficient (C) of the four-thirds flux law (Turner 1973):

$$\alpha F_T = C(R_\rho) \left(g \frac{\kappa_T^2}{\nu} \right)^{\frac{1}{3}} (\alpha \Delta T)^{\frac{4}{3}} \quad (15)$$

The data indicate the expected tendency of the flux law coefficient to increase at lower R_ρ and higher Ri (Figure 11). The former trend is consistent with Kelly et al. (1990) and Flanagan et al. (2013) whose work did not include shear effects. The noted exception to this tendency is $R_\rho = 7$ and Ri = [5 10] case in Figure 11.

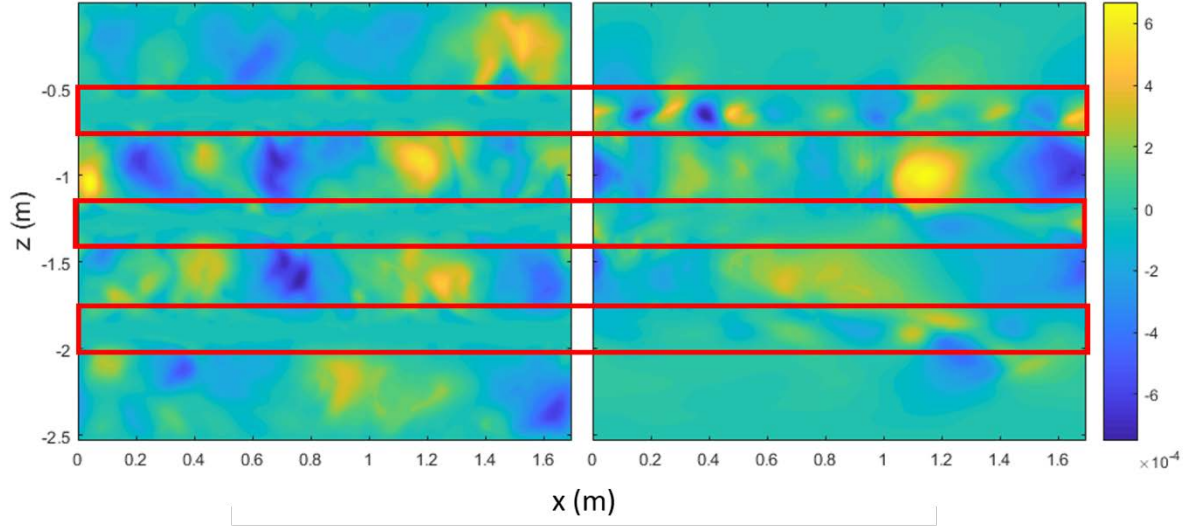


$Ri = \infty$ (*), $Ri = 40$ (+), $Ri = 10$ (.), $Ri = 5$ (x).

Figure 11. C vs. density ratio.

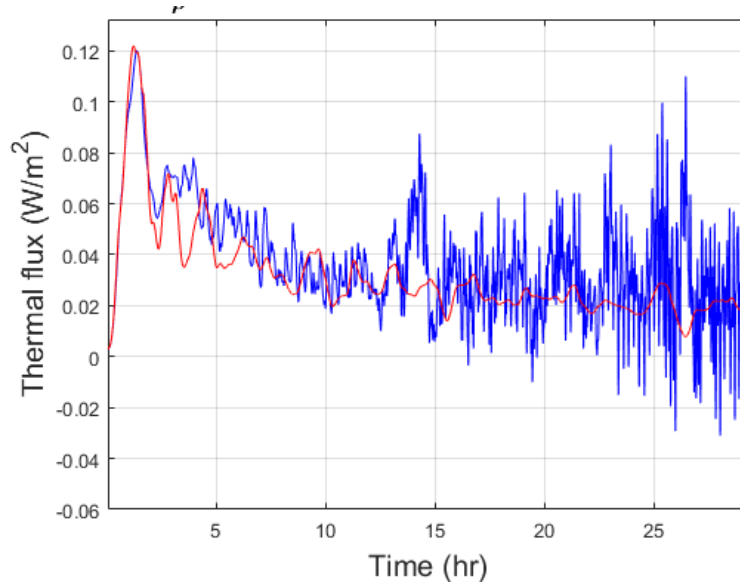
C. EFFECTS OF SHEAR ON THE LAYER STRUCTURE

The initial conditions of the simulations have a distinct staircase structure: there are four 2-m layers separated by three well-defined interfaces. Over time, salt and temperature are transported primarily by advection within the layers and by diffusion or other small-scale processes across the interfaces. For a given density ratio, shear is the only factor that differs between the simulations. Data indicate that—in the absence of shear—the interfacial transport of temperature and salt is dominated by diffusion, and no vertical motion is present. All turbulent motion occurs within the layers. When shear is applied to the simulations, the interfaces become more active, and strong turbulent motion becomes prevalent Figure 12. This turbulent motion through the interfaces leads to the interlayer advection of both heat and salt, which could be the driving force that increases the heat flux in these cases. This turbulence also leads to a large variability in the heat flux as seen in Figure 13.



W-velocity: density ratio 5 simulation with no shear (left) versus density ratio 5 simulation with shear (right), both at $t = 20$ hrs.

Figure 12. W velocity comparison.

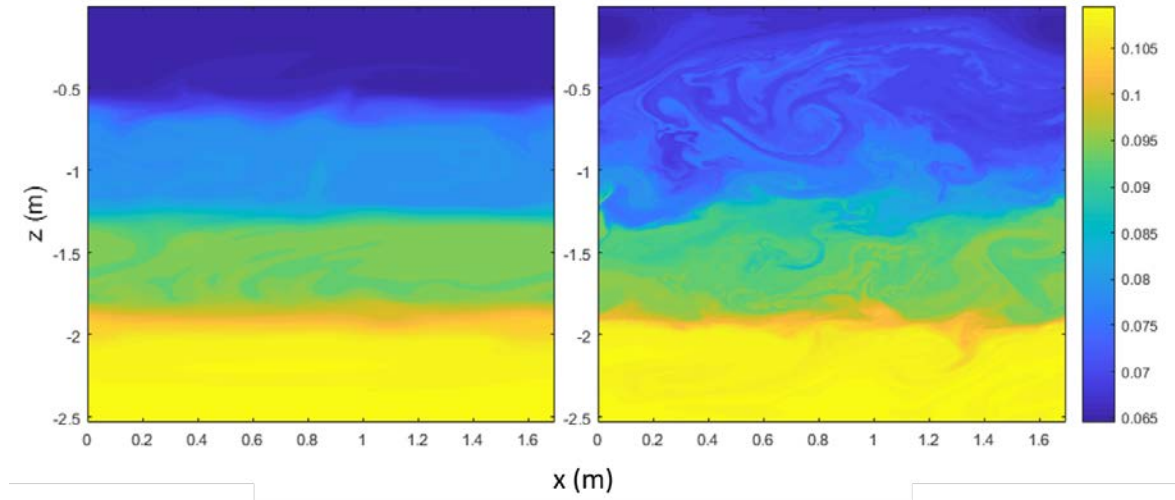


Comparison of the mean of the maximum heat flux over time between the case without shear (red) and 0.035 s^{-1} density ratio 5 case (blue).

Figure 13. Shear vs. no-shear series.

Strong shear is seen to disrupt the interfaces for large density ratios. Figure 14 compares the temperature fields for two simulations of Richardson number 5 and density

ratios of 5 (left) and 7 (right). The higher density ratio case has a greater shear to compensate for the more stable density gradient. In the case with lower density ratio, though small disturbances are present within the interfaces, the layers are still defined. For the case with larger density ratio, the top two layers and corresponding interface have been completely destroyed. With a $\gamma = 4.9613$, F_T increase from this simulation is most likely not from diffusive convection but mixing caused by the Kelvin-Helmholtz instability.



Comparison of coherent structure with temperature diffusion across three interfaces. Coherent $R_\rho = 5$; $Ri = 5$ (left) vs. disrupted structure $R_\rho = 7$; $Ri = 5$ (right).

Figure 14. Coherent vs. disrupted layers.

THIS PAGE INTENTIONALLY LEFT BLANK.

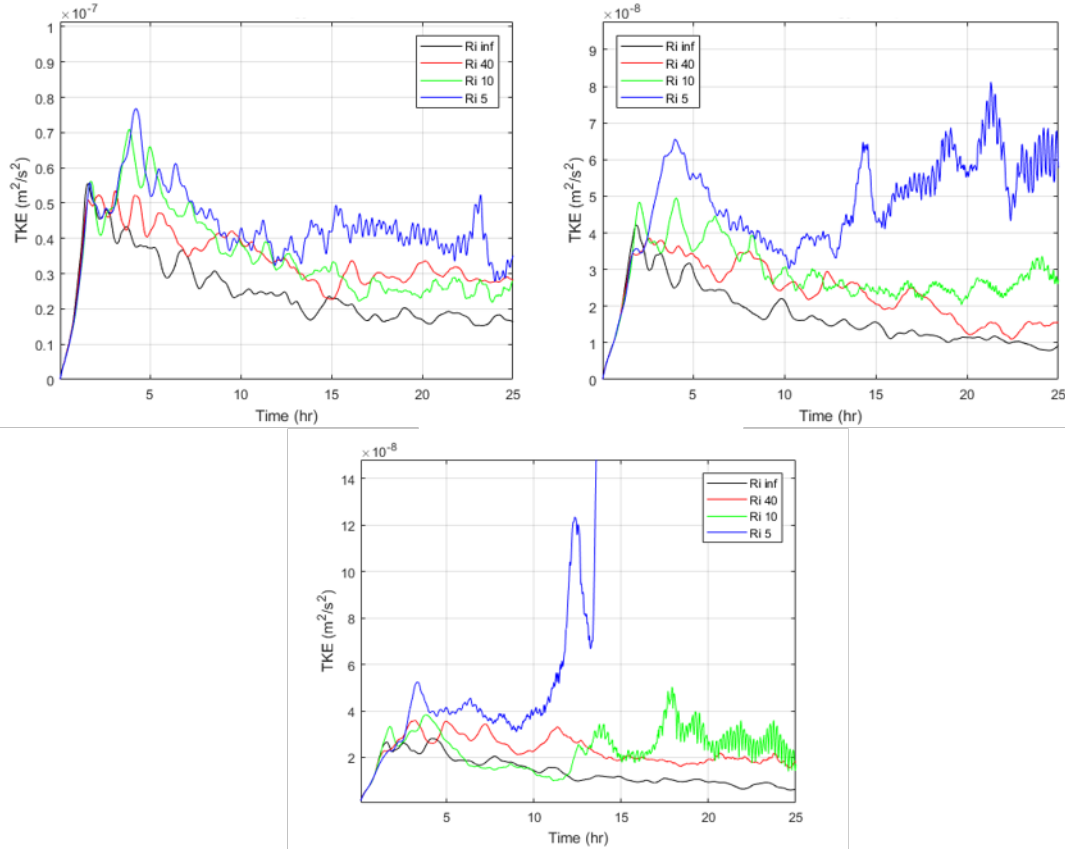
IV. RESULTS: ENERGETICS

A. CONSTANT SHEAR

The constant shear data clearly indicate that mean heat flux tends to increase as the shear rate increases, which is attributed to thermohaline-shear instability. We observe that instability does not depend only on Ri but on the density ratio as well. Therefore, the shear rate appears to play a role in the layer disruption beyond its contribution to Ri . Simulations with larger shear or velocity tend to be more unstable. In order to quantify this, we calculated the turbulent kinetic energy (TKE). By removing the background velocity, we were able to use the velocity perturbations in order to calculate the TKE of the simulations. The turbulent kinetic energy was then given by

$$TKE = \frac{1}{2}((u - \bar{u})^2 + v^2 + w^2) \quad (16)$$

which is plotted with respect to time in Figure 15.



Turbulent kinetic energy over time for constant shear regime. (top left) density ratio 3, (top right) density ratio 5, (bottom) density ratio 7.

Figure 15. TKE series: Constant shear.

A common trend through all values of the density ratio is that as the shear rate increases, the amount of energy in the system increases. The increased energy into the system is likely related to the turbulent motion at the interfaces seen in the $Ri = 5$ case shown in Figure 12. That motion led to an increased turbulent mixing of the layers. Therefore, higher shear rates may be the cause of the disrupted layers which result in the turbulent mixing of the layers leading to a temporary increased heat flux.

B. OSCILLATING SHEAR

This analysis was then applied to the oscillating shear simulations; however, the physics of such cases appear to be more complex. Figure 16 displays the no-shear simulation in black and the oscillating-frequency simulations from inertial to buoyancy

labeled as A–D. The measured TKE for these simulations do not follow the same trend as above. The most energetic simulation resulted in the lowest F_T . The reason for the large increase in TKE without an associated increase in heat flux is due to the oscillating shear exciting internal waves in the system that led to strong vertical motion but little net heat transport.

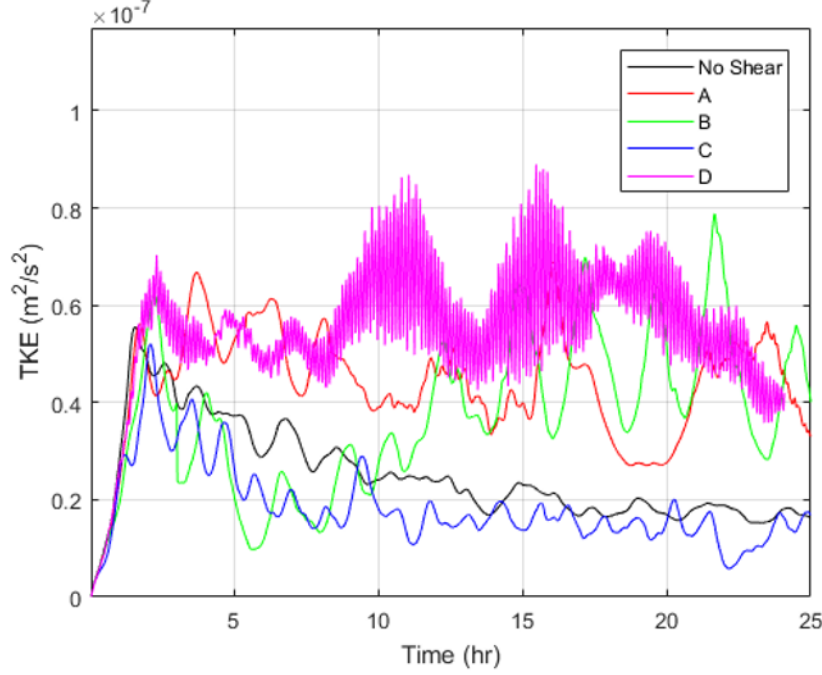
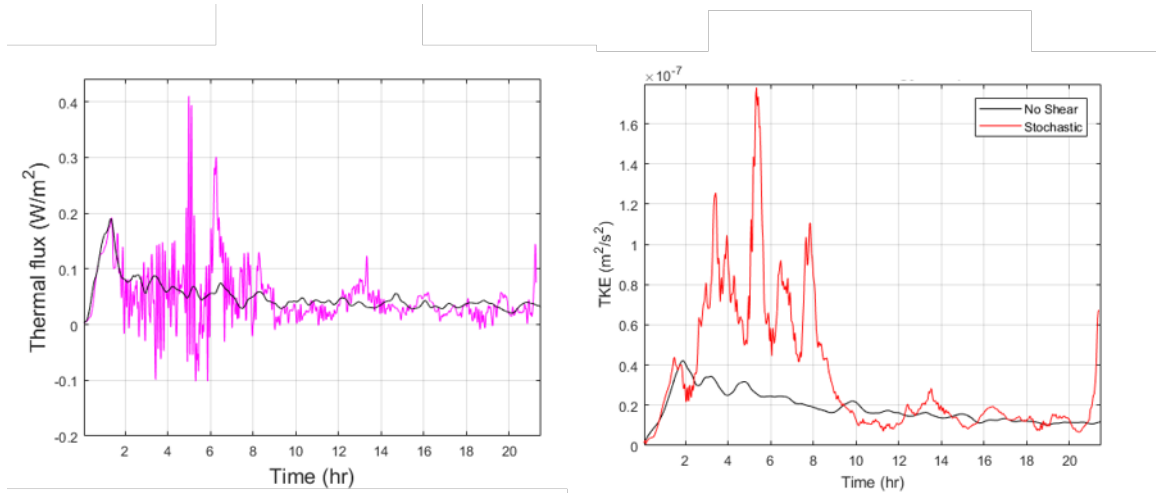


Figure 16. TKE series: Oscillating shear.

C. STOCHASTIC SHEAR

The TKE measured from the stochastic simulation behaved similarly to the oscillating cases with large perturbation energy due to the presence of internal waves. As mentioned in Chapter III, the stochastic shear simulation did not lead to a significant change in mean F_T . The TKE, as shown in Figure 17, is largest for the same duration of strong oscillations in the thermal flux indicative of internal waves. In most cases, large shear rates lead to increased kinetic energy, which therefore promotes heat flux. If the shear oscillates, internal waves are excited, which do increase the kinetic energy but do not appear to affect average thermal flux or layer structure substantially.



Stochastic simulation. Heat flux (left) TKE (right).

Figure 17. Stochastic simulation.

V. SUMMARY

A. CONCLUSIONS

Vertical shear affects the heat flux produced through diffusive convection in the Arctic thermohaline staircases. The heat transport is sensitive to the magnitude and temporal frequency of shear and, depending on the circumstances, shear can increase or decrease the heat flux of diffusive convection. The Richardson number plays a significant role in determining the heat flux through diffusive layers, with lower Richardson numbers leading to an increase in F_T . For low Ri and large density ratio, there is a transition from diffusive layers to the development of the Kelvin–Helmholtz instability which eventually collapses the staircase structure. This led to the conclusion that the energy injected into the system from the velocity may have caused turbulent conditions at the interfaces, thereby creating additional mixing of the system.

Although the majority of the oscillating simulations indicate an increase in F_T as compared to a no-shear case with same density ratio, the data indicate that at lower oscillation frequencies, the magnitude of the increase is greater than those of the higher frequencies. For these cases, the TKE did not correlate with the heat flux, particularly for those with higher frequencies of oscillation due to the oscillations triggering internal waves. We also performed a single stochastic simulation, which contained a spectrum of oscillation frequencies. Large oscillations in F_T analogous to those present in the high frequency simulations of the oscillating-shear case also suggest the presence of internal waves. The temporal heat flux pattern had a strong correlation with the TKE in the stochastic simulation. However, the mean F_T did not change significantly relative to the mean flux in the no-shear simulation for the time frame evaluated. Similar to the single-frequency oscillating simulations, F_T rapidly changed signs, leading to a negligible mean F_T change. Lastly, in the 3D shear simulation had a 30% heat flux increase as compared to the 2D simulation with the same parameters.

The introduction of shear had a noticeable effect throughout all the simulations on the structure of the thermohaline staircases. When shear was applied to the system, the

interfaces between the layers became turbulent, which is unlike the typical quiescent nature of diffusive convection interfaces. With the exception of the $R_\rho = 7$, $Ri = 5$ simulation which led to disruption of the layers, that motion could be the reason for the small increases in F_T throughout the majority of the sheared simulations.

Laboratory-based no-shear heat transport estimates as listed in Figure 2, show that double diffusive convection adds approximately $0.22 \frac{W}{m^2}$ heat transport to the sea ice in the Arctic Ocean. Numerical no-shear simulations (Flanagan et al. 2013) suggest even higher values of $0.4 \frac{W}{m^2}$. The addition of shear's contribution to that heat flux, depending on the shear regime, may be significant enough to increase that value by 20–30%. According to Kwok and Untersteiner (2011), the addition of approximately $1 \frac{W}{m^2}$ can explain why the sea ice is melting at its current rate. This shows that double diffusive convection's contribution is substantial and the increase provided by shear only adds to the significance. Since it is the goal of every environmental prediction system to present the most accurate forecast, the diapycnal mixing driven by a combination of shear and diffusive convection should be taken into account in operational and climate Arctic models. The results from this paper may assist in a more accurate and precise predictive models for projecting when the Arctic may be sea ice free.

B. RECOMMENDATIONS

This research is the initial attempt to diagnose the effect of vertical shear on the heat flux produced through the Arctic staircases. There are plenty opportunities to build upon this work. The oscillating simulations in this research were restricted to one specific density ratio. Future studies could incorporate a range of density ratios exploring a wider range of frequencies that could lead to a more refined mean heat flux model. Additionally, using an analytic model of the shear dependence of diffusive convection could be implemented into a larger circulation model. Lastly, the effects of three-dimensionality could be explored for high-density ratios and low Richardson numbers in order to investigate the transition from thermohaline instability to Kelvin-Helmholtz instability.

LIST OF REFERENCES

- Adcroft, A. J., C. N. Hill, and J. C. Marshall, 1999: A new treatment of the Coriolis terms in C grid models at both high and low resolutions. *Monthly Weather Review*, **127**, 1928–, doi:10.1175/1520-0493(1999)127<1928:ANTOTC>2.0.CO;2.
- Adcroft, A., C. Hill, and J. Marshall, 1997: Representation of topography by shaved cells in a height coordinate ocean model. *Monthly Weather Review*, **125**, 2293–2315, doi:10.1175/1520-0493(1997)125<2293:ROTBSC>2.0.CO;2.
- Cole, S. T., M.-L. Timmermans, J. M. Toole, R. A. Krishfield, and F. T. Thwaites, 2014: Ekman veering, internal waves, and turbulence Observed under Arctic Sea ice. *J. Phys. Oceanogr.*, **44**, 1306–1328, doi:10.1175/JPO-D-12-0191.1.
- Flanagan, J. D., A. S. Lefler, and T. Radko, 2013: Heat transport through diffusive interfaces. *Geophysical Research Letters*, **40**, 2466–2470, doi:10.1002/grl.50440.
- Hill, C., and J. Marshall, 1996: Application of a parallel Navier-Stokes model to ocean circulation. *Parallel Computational Fluid Dynamics 1995*, Elsevier, 545–552.
- Kelley, D. E., 1984: Effective diffusivities within oceanic thermohaline staircases. *Journal of Geophysical Research*, **89**, 10484–10488, doi: 10.1029/JC089iC06p10484.
- Kelley, D. E., 1990: Fluxes through diffusive staircases: A new formulation. *Journal of Geophysical Research*, **95**, 3365–3371, doi: 10.1029/JC095iC03p03365.
- Kwok, R., and N. Untersteiner, 2011: New high-resolution images of summer Arctic Sea ice. *Eos*, **92**, 53–54, doi: 10.1029/2011EO070002.
- Levine, M. D., C. A. Paulson, and J. H. Morison, 1987: Observations of internal gravity waves under the Arctic pack ice. *Journal of Geophysical Research: Oceans*, **92**, 779–782, doi: 10.1029/JC092iC01p00779.
- Marshall, J., C. Hill, L. Perelman, and A. Adcroft, 1997: Hydrostatic, quasi-hydrostatic, and nonhydrostatic ocean modeling. *Journal of Geophysical Research: Oceans*, **102**, 5733–5752, doi: 10.1029/96JC02776.
- Marshall, J., H. Jones, and C. Hill, 1998: Efficient ocean modeling using non-hydrostatic algorithms. *Journal of Marine Systems*, **18**, 115–134, doi: 10.1016/S0924-7963(98)00008-6.
- Maslowski, W., J. Clement Kinney, M. Higgins, and A. Roberts, 2012: The future of Arctic Sea ice. *Annual Review of Earth and Planetary Sciences*, **40**, 625–654, doi: 10.1146/annurev-earth-042711-105345.

- Neal, V. T., S. Neshyba, and W. Denner, 1969: Thermal stratification in the Arctic Ocean. *Science*, **166**, 373–374, doi:10.1126/science.166.3903.373.
- Padman, L., and T. M. Dillon, 1987: Vertical heat fluxes through the Beaufort Sea thermohaline staircase. *Journal of Geophysical Research*, **92**, 10799, doi: 10.1029/JC092iC10p10799.
- Perovich, D. K., and B. Elder, 2002: Estimates of ocean heat flux at SHEBA. *Geophysical Research Letters*, **29**, 58–1–58–4, doi: 10.1029/2001GL014171.
- Radko, T., 2010: Equilibration of weakly nonlinear salt fingers *J. Fluid Mech.*, **645**, 121–143.
- Radko, T., 2013: Double-Diffusive Convection. Cambridge University Press, Cambridge.
- Radko, T., J. Ball, J. Colosi and J. Flanagan, 2015: Double-diffusive convection in a stochastic shear. *J. Phys. Oceanogr.*, **45**, 3155–3167.
- Smyth, W. D., and S. Kimura, 2007: Instability and momentum transport in a double-diffusive, stratified shear layer. *J. Phys. Oceanogr.*, **11**, 1551–1556.
- Stern, M. E., 1960: The “Salt-Fountain” and thermohaline convection. *Tellus*, **12**, 172–175, doi:10.1111/j.2153-3490.1960.tb01295.x.
- Stroeve, J. C., J. Maslanik, M. C. Serreze, I. Rigor, W. Meier, and C. Fowler, 2011: Sea ice response to an extreme negative phase of the Arctic oscillation during winter 2009/2010. *Geophysical Research Letters*, **38**, L02502–n/a, doi: 10.1029/2010GL045662.
- Stroeve, J., and W. Maslowski, 2008: Arctic Sea Ice variability during the last half century. *climate variability and extremes during the past 100 years*, Springer Netherlands, Dordrecht, 143–154.
- Timmermans, M.-L., J. Toole, R. Krishfield, and P. Winsor, 2008: Ice-Tethered Profiler observations of the double-diffusive staircase in the Canada Basin thermocline. *Journal of Geophysical Research*, **113**, C00A02, doi:10.1029/2008JC004829.
- Turner, J. S., 1973: *Buoyancy Effects in Fluids*. Cambridge University Press, Cambridge, pp. 367.
- Turner, J. S., 1978: Double-diffusive intrusions into a density gradient. *Journal of Geophysical Research*, **83**, 2887, doi: 10.1029/jc083ic06p02887.
- Turner, J. S., 2010: The Melting of Ice in the Arctic Ocean: The influence of double-diffusive transport of heat from below. *J. Phys. Oceanogr.*, **40**, 249–, doi:10.1175/2009JPO4279.1.

- Walın, G., 1964: Note on the stability of water stratified by both salt and heat. *Tellus*, 16, 389– 393, doi:10.1111/j.2153-3490.1964.tb00175.x.
- Wells, M. G., and J. S. Wettlaufer, 2007: The long-term circulation driven by density currents in a two-layer stratified basin. *J. Fluid Mech*, 572, 37–58, doi: 10.1017/S0022112006003478.

THIS PAGE INTENTIONALLY LEFT BLANK

INITIAL DISTRIBUTION LIST

1. Defense Technical Information Center
Ft. Belvoir, Virginia
2. Dudley Knox Library
Naval Postgraduate School
Monterey, California